DEVELOPMENT OF A 3RD-ORDER VORTICITY CONFINEMENT SCHEME FOR ROTOR WAKE SIMULATIONS

M. Costes
Email: mcostes@onera.fr
ONERA, The French Aerospace Lab, F-92190 Meudon, France

Abstract

A new 3rd-order Vorticity Confinement scheme is presented as an extension of the original VC2 scheme developed by Steinhoff for the resolution of the fluid dynamic equations. The theoretical developments are explained, and the method is tested for a 2D airfoil-vortex interaction case and the simulation of the 7A rotor in hover. The results obtained show that the new scheme combines the accuracy of the underlying 3rd-order scheme and the confinement capability of the original VC2 method.

INTRODUCTION

The computation of vortices and wakes by CFD is a difficult problem for which most of the numerical techniques fail. Numerical schemes need to be dissipative for stability, so that wake sheets and vortices are diffused much faster in the computations than what actually occurs in reality. This is a serious difficulty for rotorcraft configurations because of the importance of vortical flows which strongly affect their behaviour. In hover, the flow field around the rotor blades is driven by the wake shed below the rotor. As a result, this flight configuration presents a maximum of induced power. Accurate simulation of these induced effects is thus required when trying to optimize rotor performance in hover. At low forward speed, the main rotor blades interact with their wakes. This is at the source of vibrations and more importantly of blade-vortex interactions and BVI noise, especially in descent flight. Again, the capability to simulate BVI requires a good capture of the wake vortices and their convection until they encounter a following blade. The main rotor wake also interacts with the airframe, especially the tail surfaces. Therefore properly accounting for wake interactions is crucial when considering the flight dynamics of the helicopter, particularly at low-speed.

This explains why the rotorcraft community has been particularly concerned with the wake capturing properties of numerical methods. A large part of the methods applied in the past use a Lagrangian approach, which allows a perfect conservation of the wake sheets. However, most of them are inviscid, incompressible, and have difficulties to deal with the merging of vortical structures. The Eulerian approach is more general and has been favoured more recently, following the progress of CFD. A significant amount of work has been done in this field, considering either automatic mesh adaptation in order to concentrate the mesh points in the vicinity of the vortices or the application of higher-order discretizations. The objective of both approaches is to reduce numerical diffusion and limit the artificial spreading of the wakes, but this diffusion cannot be totally removed. In the Eulerian framework, other alternative techniques have also been proposed, among which the Vorticity Confinement method of Steinhoff [1], which proved to be very efficient for wake conservation. Such a method has been investigated at ONERA, considering first simple problems for which a deep analysis can be done [2, 3]. We are more particularly interested here in the second VC scheme proposed by Steinhoff, known as VC2 [4, 5]. In spite of its efficiency, the original VC formulation is only 1st-order accurate, the internal profile of the confined vortices being rapidly governed by the VC term. In a follow-on work [6], higher-order confinement schemes were developed for the linear transport equation. The main outcome of this study is that all schemes asymptotically converge towards the same confined solution, but the rate of convergence towards the asymptotic solution depends on the order of the scheme. As a result, higher-order confinement takes benefit of both the negative dissipation of the scheme and its higher accuracy. In parallel to that, rotorcraft applications of the original VC2 scheme were considered [7].

The topic of the present paper is the extension of the 3rd-order VC scheme developed in [6] to the Euler/RANS equations and to apply it to helicopter-related problems. In a first part of the paper, the theoretical developments are presented, starting with a brief reminder of the basic 3rd-order confinement scheme for the linear 1D transport equation, and then explaining how it is extended to the CFD equations. The following part of the paper presents two applications of the method: a 2D airfoil-vortex interaction case and the 3D case of the 7A rotor in hover. The first application is computed on very fine grids in order to check the consistency of the confined solutions with the fluid dynamic equations and to evaluate the benefit of higher-order confinement. The objective of the second case is to demonstrate the applicability of the new method to helicopter problems.

THEORETICAL DEVELOPMENTS

1D Linear Transport Equation

The VC methodology was developed by Steinhoff et al based on the theory of Nonlinear Solitary Waves. We adopt a different approach here, leading to similar results. Consider the simple case of the 1D transport equation:

$$\frac{\partial u}{\partial t} + c\frac{\partial u}{\partial x} = 0 \qquad (1)$$

with $c > 0$ is a constant transport speed of a quantity $u \geq 0$. The original VC2 term uses a 2nd-difference of the harmonic mean between two successive grid values to correct the highly-diffusive 1st-order discretization of the equation, so that (1) can be discretized by:

$$u_j^{n+1} = u_j^n - \sigma\left(u_j^n - u_{j-1}^n\right) - \varepsilon\frac{\sigma(1-\sigma)}{2}\left(h\left(u_{j+1}^n, u_j^n\right) - 2h\left(u_j^n, u_{j-1}^n\right) + h\left(u_{j-1}^n, u_{j-2}^n\right)\right) \qquad (2)$$

with

$\sigma = \frac{c\Delta x}{\Delta t}$ the CFL number,

$$h\left(u_j^n, u_{j+1}^n\right) = \begin{cases} \dfrac{2u_j^n u_{j+1}^n}{u_j^n + u_{j+1}^n} & \text{if } \operatorname{sgn}\left(u_j^n\right) = \operatorname{sgn}\left(u_{j+1}^n\right) \\ 0 & \text{elsewhere} \end{cases}$$

the harmonic mean,

$\varepsilon \geq 1$ the confinement parameter.

The VC2 term, second line of (2), therefore writes:

$$-\varepsilon \frac{\sigma(1-\sigma)}{2} \delta^2 h\left(u_{j-1}^n, u_j^n\right) \tag{3}$$

Deriving the equivalent partial differential equation from the linear differences of (2) and leaving the harmonic mean term unmodified leads to a mixed differential/difference equation representative of the numerical problem which we actually solve:

$$\frac{\partial u}{\partial t} + c\frac{\partial u}{\partial x} - c\Delta x \frac{(1-\sigma)}{2}\left[\frac{\partial^2 u}{\partial x^2} - \varepsilon \frac{\delta^2 h(u)}{\Delta x^2}\right] = 0 \tag{4}$$

When $u \neq 0$, a Taylor expansion of the 2nd difference of the harmonic mean can be done, giving the leading term of the truncation error:

$$-(\varepsilon - 1)c\Delta x \frac{(1-\sigma)}{2}\frac{\partial^2 u}{\partial x^2} \tag{5}$$

For $\varepsilon > 1$, negative dissipation is introduced and the corresponding scheme, although 1st-order accurate, has the capability to conserve indefinitely non-trivial solutions which are transported at the correct speed by the numerical scheme. As shown in [6], the corresponding pulse solutions are obtained by balancing the numerical diffusion of the first-order scheme and the nonlinear confinement term at the discrete level. Finally, it is important to remark that if the VC2 term (3) is replaced by any linear second-difference in (2), stability requires $\varepsilon = 1$. Since the leading term in the Taylor series development is identical between the nonlinear VC2 and any linear 2nd-difference, (5) shows that the linear schemes are 2nd-order accurate. According to the stencil used, the well-known Lax-Wendroff, Warming-Beam and Fromm scheme can be obtained. The leading term in the truncation error has a 3rd derivative and is dispersive. Further, all these linear schemes are dissipative with a leading dissipative term given by the 4th derivative in their Taylor expansion. As a result, they asymptotically converge towards trivial solutions equal to a constant value and therefore the initial information is almost totally lost.

The VC2 scheme was extended to higher odd orders in [6], using the same ideas of applying a non-linear approximation of the opposite of the leading dissipative term of the truncation error, multiplied by a confinement parameter greater than 1 in order to render the scheme globally anti-diffusive. For 3rd-order accuracy, the discretization becomes:

$$\begin{aligned} u_j^{n+1} &= u_j^n - \sigma\left(u_j^n - u_{j-1}^n\right) - \frac{\sigma(1-\sigma)}{2}\left(u_{j+1}^n - 2u_j^n + u_{j-1}^n\right) \\ &+ \frac{(1+\sigma)\sigma(1-\sigma)}{6}\left(u_{j+1}^n - 3u_j^n + 3u_{j-1}^n - u_{j-2}^n\right) \\ &+ \varepsilon \frac{(1+\sigma)\sigma(1-\sigma)(2-\sigma)}{24}\left[h\left(u_{j+1}^n, u_{j+2}^n\right) - 4h\left(u_j^n, u_{j+1}^n\right)\right. \\ &\left. + 6h\left(u_{j-1}^n, u_j^n\right) - 4h\left(u_{j-2}^n, u_{j-1}^n\right) + h\left(u_{j-3}^n, u_{j-2}^n\right)\right] \end{aligned} \tag{6}$$

The 3rd-order VC term is now (last 2 lines of (6)):

$$+\varepsilon \frac{(1+\sigma)\sigma(1-\sigma)(2-\sigma)}{24}\delta^4 h\left(u_{j-1}^n, u_j^n\right) \tag{7}$$

The leading term in the truncation error is also:

$$+(\varepsilon - 1)c\Delta x^3 \frac{(1+\sigma)(1-\sigma)(2-\sigma)}{24}\frac{\partial^4 u}{\partial x^4} \tag{8}$$

When $\varepsilon > 1$, we have again negative dissipation ensuring the confinement property of this 3rd-order accurate scheme. In [6], we showed that these VC schemes extended to any order have the same asymptotic pulse solutions which can be transported exactly at the discrete level. The interest of the higher-order schemes is that any initial solution converges slower to this asymptotic solution so that the benefits of higher-accuracy and of confinement can be combined.

Extension to the Euler/RANS Equations

Extending the VC2 schemes to the Euler/RANS equations is not straightforward because vorticity is not part of the conservative variables generally used in their resolution. In order to see how to translate the discretization from the linear transport equation to CFD, we will use the original formulation of the VC2 scheme. As described by Steinhoff, the VC term is included in the momentum equation as a source term:

$$\frac{d\vec{U}}{dt} + \frac{1}{\rho}\vec{\nabla}p - \frac{1}{\rho}\vec{\nabla}\cdot\overline{\overline{\tau}} = \vec{f} \tag{9}$$

with:

$$\vec{f} = -\vec{\nabla}\times\left(\mu\vec{\omega} - \varepsilon\vec{w}\right) \tag{10}$$

The first term in (10) is the vorticity vector, while the second one is aligned with vorticity, and its magnitude is equal to the harmonic mean of the vorticity modulus of the surrounding grid points, giving:

$$\vec{w} = \frac{\vec{\omega}}{\omega}\left[\frac{\sum_{l=1}^{N}(\omega_l)^{-1}}{N}\right]^{-1} = h(\omega_1 \ldots \omega_N)\frac{\vec{\omega}}{\omega}$$

The link between (10) and (3) requires a derivation of the vorticity transport equation, which is obtained by taking the curl of the momentum equation (9). We use a modified version of it for the specific vorticity in order to get rid of compressibility terms, giving:

$$\begin{aligned} &\frac{d}{dt}\left(\frac{\vec{\omega}}{\rho}\right) = \frac{\partial}{\partial t}\left(\frac{\vec{\omega}}{\rho}\right) + \vec{U}\cdot\vec{\nabla}\left(\frac{\vec{\omega}}{\rho}\right) = \\ &\overline{\overline{\nabla\vec{U}}}\cdot\frac{\vec{\omega}}{\rho} - \frac{1}{\rho}\vec{\nabla}\times\left(\frac{\vec{\nabla}p}{\rho}\right) + \frac{1}{\rho}\vec{\nabla}\times\left(\frac{\vec{\nabla}\cdot\overline{\overline{\tau}}}{\rho}\right) + \frac{1}{\rho}\vec{\nabla}\times\vec{f} \end{aligned} \tag{11}$$

For an isolated 2D vortex in inviscid flow, all terms except the last one on the right hand side of (11) vanish, allowing great simplifications of the equation. The VC term indirectly appears in the vorticity transport equation as:

$$\vec{\nabla}\times\vec{f} = \vec{\nabla}^2\left(\mu\vec{\omega} - \varepsilon\vec{w}\right) - \vec{\nabla}\left(\vec{\nabla}\cdot\left(\mu\vec{\omega} - \varepsilon\vec{w}\right)\right) \tag{12}$$

Again, the second term is equal to zero for an isolated 2D vortex, so that the vorticity transport equation can be written, for a 2D vortex in inviscid flow:

$$\frac{\partial}{\partial t}\left(\frac{\omega}{\rho}\right) + \vec{U}\cdot\vec{\nabla}\left(\frac{\omega}{\rho}\right) - \frac{1}{\rho}\nabla^2\left(\mu\omega - \varepsilon h(\omega)\right) = 0 \tag{13}$$

The analogy of (13) with (4) is now clear. The first term of (10) is a diffusion term, which mimics the effect of the truncation error of the linear differences in (2). This contribution was found helpful for prescribing a linear

diffusion term independently of the numerical scheme used. The second term in (10) is the anti-diffusive confinement term. The user-prescribed parameters, μ and ε, are both set proportional to the mesh size Δx for consistency. Finally, the ratio ε/μ is the equivalent of the value of the confinement parameter ε for the linear transport equation.

At 3rd-order, we want to introduce the equivalent of the 4th-difference (7) in the vorticity transport equation. The idea is that, exactly as the 4th-difference in (7) can be obtained by recursively applying 1st-differences to the harmonic mean $h\left(u_{j-1}^n, u_j^n\right)$ 4 times, applying the curl operator twice to the original VC term will naturally increase the order of the differencing by 2 since most of the terms disappear, leaving higher-order derivatives only:

$$\begin{aligned} &\vec{a} = \varepsilon\vec{w} - \mu\vec{\omega} \\ &\vec{f} = \vec{\nabla}\times\vec{a} \\ &\vec{\nabla}\times\vec{f} = \vec{\nabla}\left(\vec{\nabla}\cdot\vec{a}\right) - \vec{\nabla}^2\vec{a} \\ &\vec{\nabla}\times\left(\vec{\nabla}\times\vec{f}\right) = -\vec{\nabla}\times\left(\vec{\nabla}^2\vec{a}\right) \end{aligned} \tag{14}$$

An interesting property of the Laplacian is that it is rotationally invariant, following the same ideas used by Steinhoff in the development of the VC method. Because our model equation is the vorticity transport equation, we are interested by the curl of the new confinement term, equal to:

$$\vec{\nabla}\times\left(\vec{\nabla}\times\left(\vec{\nabla}\times\vec{f}\right)\right) = -\vec{\nabla}\left(\vec{\nabla}\cdot\left(\vec{\nabla}^2\vec{a}\right)\right) - \vec{\nabla}^2\left(\vec{\nabla}^2\vec{a}\right) \tag{15}$$

As for the original VC2 case, the first term on the right hand side of (15) vanishes for a 2D isolated vortex, and the added confinement term is fully similar to (7), with the sum of a diffusion and a confinement term. In order to increase the order of the discretization, it suffices to use undivided differences in the computation of the Laplacian of the components of the original VC2 term, giving:

$$\vec{f} = \vec{\nabla}\times\left(\mu\vec{\delta}^2\vec{\omega} - \varepsilon\vec{\delta}^2\vec{w}\right) \tag{16}$$

Since the original VC2 scheme is 1st-order accurate, (16) is now 3rd-order accurate.

Practically, the regions of the flow field where the confinement term is applied are selected by a filter. In all our applications, the Q criterion was used for filtering the vortical regions to confine.

Numerical method

The new 3rd-order VC2 scheme was implemented in the Cassiopée Cartesian solver of the elsA suite, in which the original version of VC2 had already been implemented previously. Besides the centered 2nd-order space discretization with Jameson's artificial viscosity terms, the Cassiopée solver also has centered non-compact 3rd-order and 5th-order directional schemes. The idea is to get the capability to use VC together with higher-order schemes. Since we are interested in the 3rd-order confinement, we just present the 3rd-order discretization here, developed by Saunier et al in [8]. Thanks to the equivalence between the finite-volume and finite-difference approach on Cartesian grids, it can be greatly simplified with respect to curvilinear grids, writing in the case of the 2D Euler equations:

$$W_t + \frac{\delta_1}{\Delta x}\left(I - \frac{1}{6}\delta_1^2\right)\mu_1 F + \frac{\delta_2}{\Delta y}\left(I - \frac{1}{6}\delta_2^2\right)\mu_2 G = 0$$

W is the vector of conservative variables, F and G are the flux vectors along the x and y directions respectively, and:

$$\begin{aligned} \left(\mu_1 F\right)_{j+1/2,k} &= \frac{1}{2}\left(F_{j+1,k} + F_{j,k}\right) \\ \left(\delta_1 F\right)_{j+1/2,k} &= F_{j+1,k} - F_{j,k} \\ \left(\mu_2 G\right)_{j,k+1/2} &= \frac{1}{2}\left(G_{j,k+1} + G_{j,k}\right) \\ \left(\delta_2 G\right)_{j,k+1/2} &= G_{j,k+1} - G_{j,k} \end{aligned}$$

are the classical averaging and difference operators along the grid directions. The corresponding 4th-order scheme is not dissipative and the classical artificial viscosity terms of Jameson are added to the flux terms. Since these last terms are 3rd-order accurate on smooth solutions, a 3rd-order accurate scheme is obtained. The vorticity confinement term (16) is added to the right hand side of the momentum equation, using standard 2nd-order finite-differences:

$$\left(\vec{\delta}^2\vec{w}\right)_l = \left(\delta_1^2 + \delta_2^2\right)w_l$$

As for the original one, the new VC method was implemented in the Cartesian solver only. To compute the flow around obstacles, curvilinear body grids are required and the Chimera overset grids method is used. For all computations presented below, a standard 2nd-order finite-volume scheme is used on the curvilinear meshes. In the Cartesian part of the simulation, both 2nd- and 3rd-order schemes have been used for comparison. The associated Chimera interpolation and VC2 schemes are consistent with the order of the Cartesian scheme, i.e. 2nd-order interpolation and the original VC2 scheme are used with the 2nd-order Cartesian scheme, and 3rd-order interpolation and 3rd-order VC2 are used with the 3rd-order Cartesian scheme.

APPLICATIONS

2D Blade-Vortex Interaction

The first configuration considered is a 2D airfoil-vortex interaction case which was already computed by Peron et al in the frame of the ONERA-JAXA cooperation [9]. This 2D Euler simulation aims at reproducing the conditions encountered by a blade section located at r/R=87.6% of the blade in the experiment of Kitaplioglu and Caradonna [10, 11]. The corresponding NACA0012 airfoil is set at 0° incidence with a freestream Mach number M_∞=0.626. A vortex is introduced in the initial flow field 10 chords upstream of the airfoil and ¼-chord below it. The interaction phase is computed until the vortex would be advected 10 chords downstream the airfoil at the freestream velocity. The non-dimensional time, normalized by chord to freestream velocity ratio, thus varies between t=-10 and t=+10, so that at t=0 the vortex is approximately located at the leading edge of the airfoil. The same Scully vortex model used in [9] was applied, with a core radius equal to 16.2% of the airfoil chord. The three sets of ONERA grids used in [9] were also tested in the present work. For each of them, the Cartesian background grid is split into three zone levels. The finest zone covers the full vortex path in the simulation, including the interaction with the airfoil. An intermediate set of zones ensures transition with the outer coarser meshes. The cell size ratio between two successive grid levels is equal to 3, and all zones communicate with Chimera interpolation. Finally, the curvilinear mesh around the airfoil is embedded in the finest level region. A view of the coarser mesh used in these computations, including the computed vorticity field for a reduced time equal to t=-9.5, is presented in Figure 1, with a detailed view of the incoming vortex and of the

airfoil regions. This mesh includes a total number of 227975 cells with about 12 of them across the vortex core. The medium mesh is twice as fine as the coarse one, including 842777 cells and 24 of them across the vortex core. Similarly, the fine mesh has a total number of 3284675 cells with 48 of them across the vortex core. These grids are therefore quite fine, but the goal here is to check that the VC2 schemes, original and 3rd-order, behave correctly when the vortex structure is well discretized.

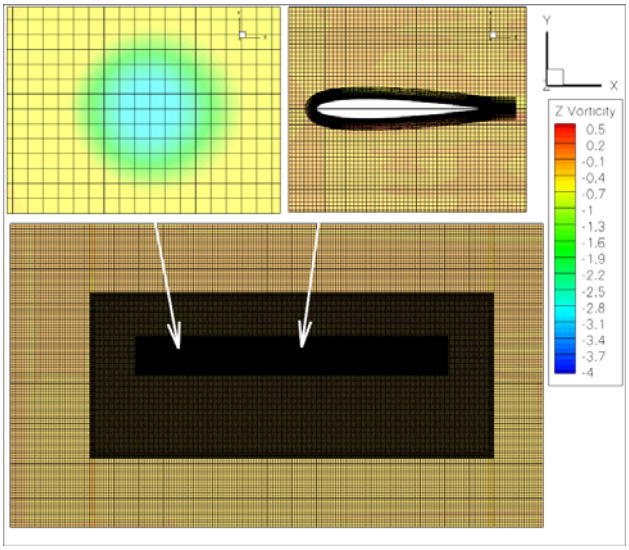

Figure 1: View of the coarse grid system with details of the Scully vortex and of the airfoil mesh at t=-9.5

The resolution in time uses a 2nd-order backward implicit discretization. The corresponding Gear equation is solved by LU factorization and a maximum number of 10 Newton iterations at each time step. The number of physical time steps used for the coarse mesh resolution is equal to 2000. The same maximum CFL number was kept for the resolution on the other grids, so that 4000 and 8000 time steps were used for the medium and the fine mesh respectively. Selecting the value of the confinement parameters is not trivial and is discussed below, based on the experience gained with the 1D linear transport equation. In the first set of computations considered, these parameters are identical in all simulations, with ε=0.02Δx and ε/μ=1.25. The vorticity profile evolution during the advection phase of the vortex ahead of the airfoil is presented in Figure 2 for the original VC2 scheme and in Figure 3 for the 3rd-order VC2, and compared with the results obtained without confinement. The solutions on the three sets of meshes are presented. For the coarse mesh, the original and 3rd-order VC2 provide sharper vorticity profiles than the corresponding solutions without confinement. However, the 2nd-order solutions show a reduction of peak vorticity of about 29% with confinement and 36% without confinement during the advection phase, while the 3rd-order scheme gives a reduction of 13% of peak vorticity without confinement and an increase by 9% of this peak vorticity when the VC2 is applied. Such an increase of peak vorticity is typical of confinement methods which asymptotically converge towards their prescribed vorticity profile resulting from the balance between the confinement term and the diffusion introduced explicitly by the μ parameter and that due to the numerical scheme with the artificial viscosity term. This effect is clear for the original VC2 scheme with the medium mesh, for which the computation with confinement gives a 36% increase of peak vorticity, while the standard 2nd-order scheme reduces the peak vorticity of 0.7% only and therefore ensures a good preservation of the vortex during the advection phase. Such large increase of peak vorticity does not appear anymore for the fine grid solution, where the 2nd-order scheme with the original VC2 increases the peak vorticity by 10% only, and the 2nd-order scheme alone by 2.6%. This nonlinear behaviour of the confinement is an illustration of the difficulty of prescribing a confinement term which ensures a good preservation of the vortex whatever the mesh refinement can be, more especially when non-linear artificial viscosity is added to the confinement terms. On the whole, the results obtained on the 3 sets of grids with the same confinement parameters are satisfactory. From this point of view, the 3rd-order VC2 scheme behaves better with mesh refinement, without large rise of the peak vorticity obtained during the advection phase. Further, a fairly good preservation of the vortex structure is obtained for all grids. When the basic scheme without confinement allows a good preservation of the vortex, the 3rd-order VC2 term hardly modifies the solution, so that the new scheme combines the benefits of the higher order discretization with the anti-diffusive property of confinement. This observation is in conformity with what could be observed with higher-order confinement schemes for the 1D linear transport equation in [6].

The confined solution is obviously dependent on the choice of the confinement parameters, mainly that of the ε/μ ratio which drives the asymptotic evolution of the solution in the absence of any other dissipation in the numerical scheme. The artificial viscosity required for stability is another nonlinear dissipative term affecting the solution, but its effect is difficult to predict. The introduction of the diffusion term in (10) or (16) aims at minimizing the influence of the numerical dissipation of the underlying scheme without confinement, provided the value of μ be high enough, although it must remain in a reasonable range of magnitudes in order to be consistent with the Euler/RANS equations. In order to check this, the same computations were completed doubling the magnitude of the confinement parameters. A comparison of both vorticity profiles is presented in Figure 4 for the 2nd-order scheme and in Figure 5 for the 3rd-order scheme. As could be expected, a higher magnitude of the confinement parameters increases the peak vorticity of the vortex during the advection phase, more especially when the coarse mesh is used. It is assumed that the larger the confinement parameters, the faster the vortex solutions will get close to their asymptotic state, which may explain the results obtained here. Once again, the lower sensitivity of the 3rd-order confinement than that of the original VC2 scheme to a variation of the numerical parameters can be noted, because of its scaling in Δx^3 instead of Δx. In general, the results obtained during the advection phase are satisfactory.

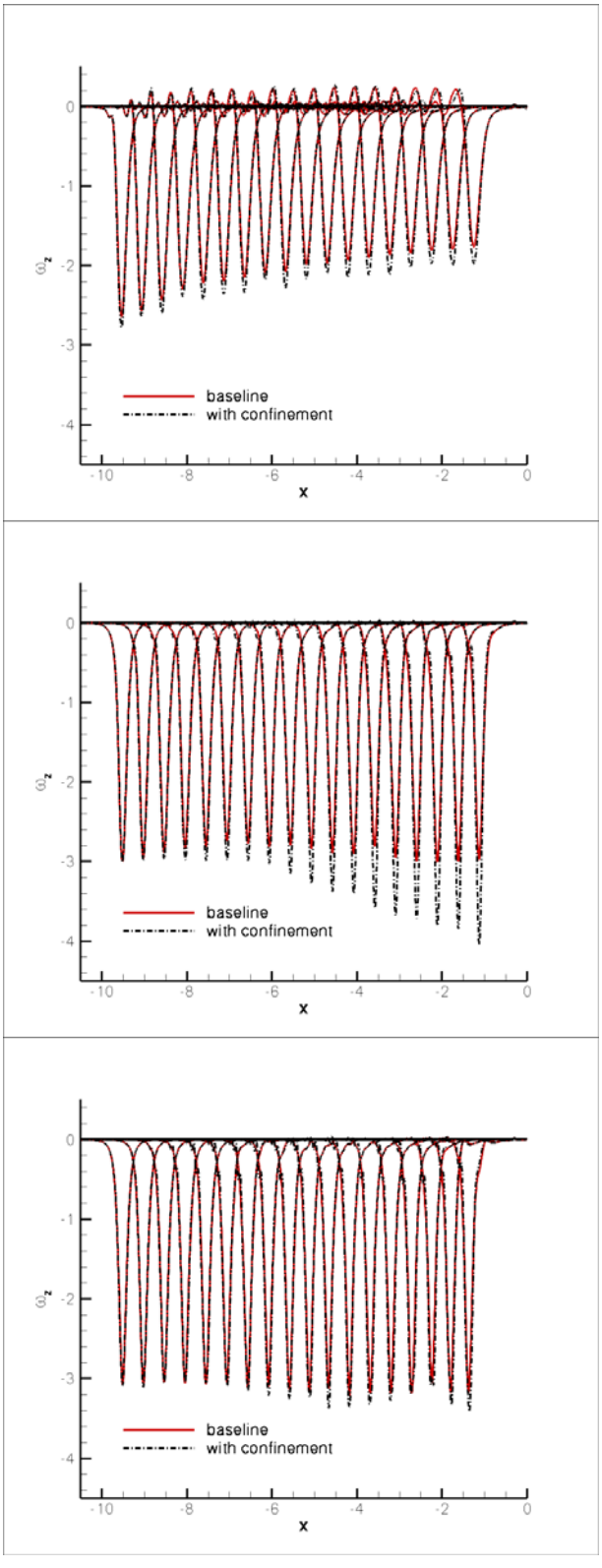

Figure 2: Vorticity profile across the vortex before the interaction with and without the original VC2 scheme – ε=0.02Δx, ε/μ=1.25– coarse mesh (top) – medium mesh (middle) – fine mesh (bottom)

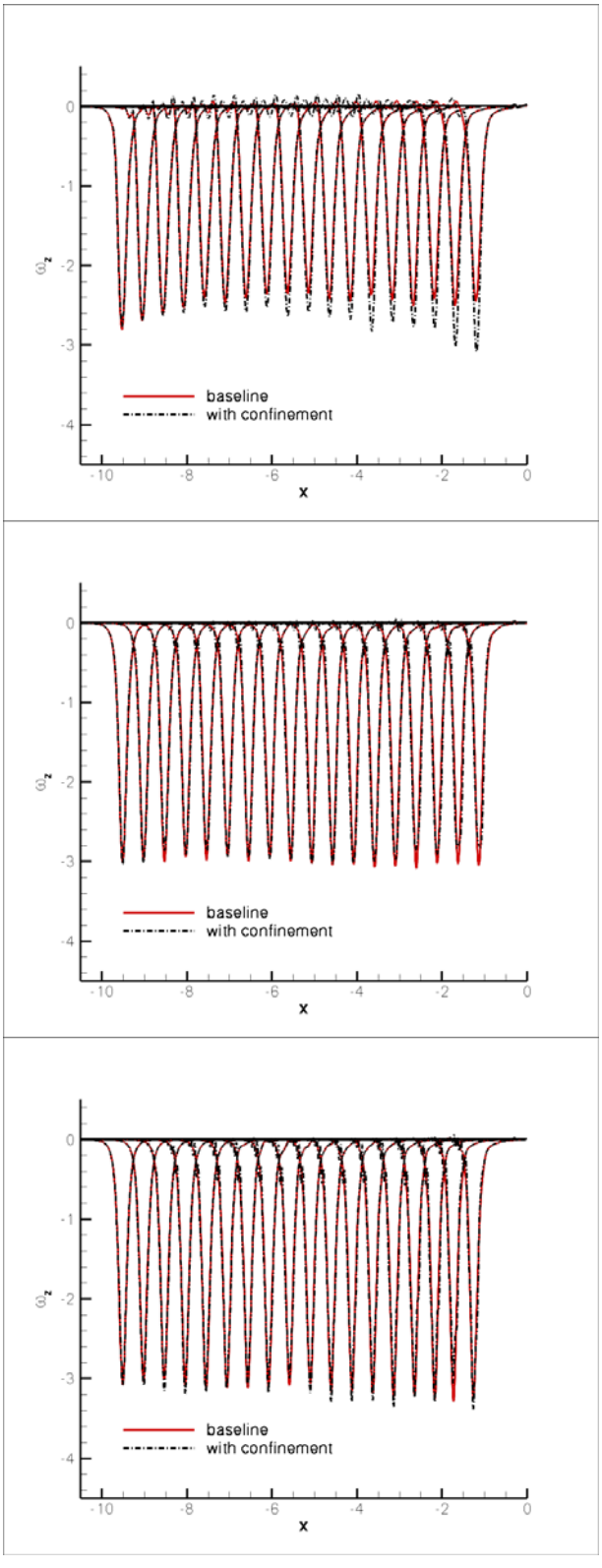

Figure 3: Vorticity profile across the vortex before the interaction with and without the 3rd-order VC2 scheme – ε=0.02Δx, ε/μ=1.25– coarse mesh (top) – medium mesh (middle) – fine mesh (bottom)

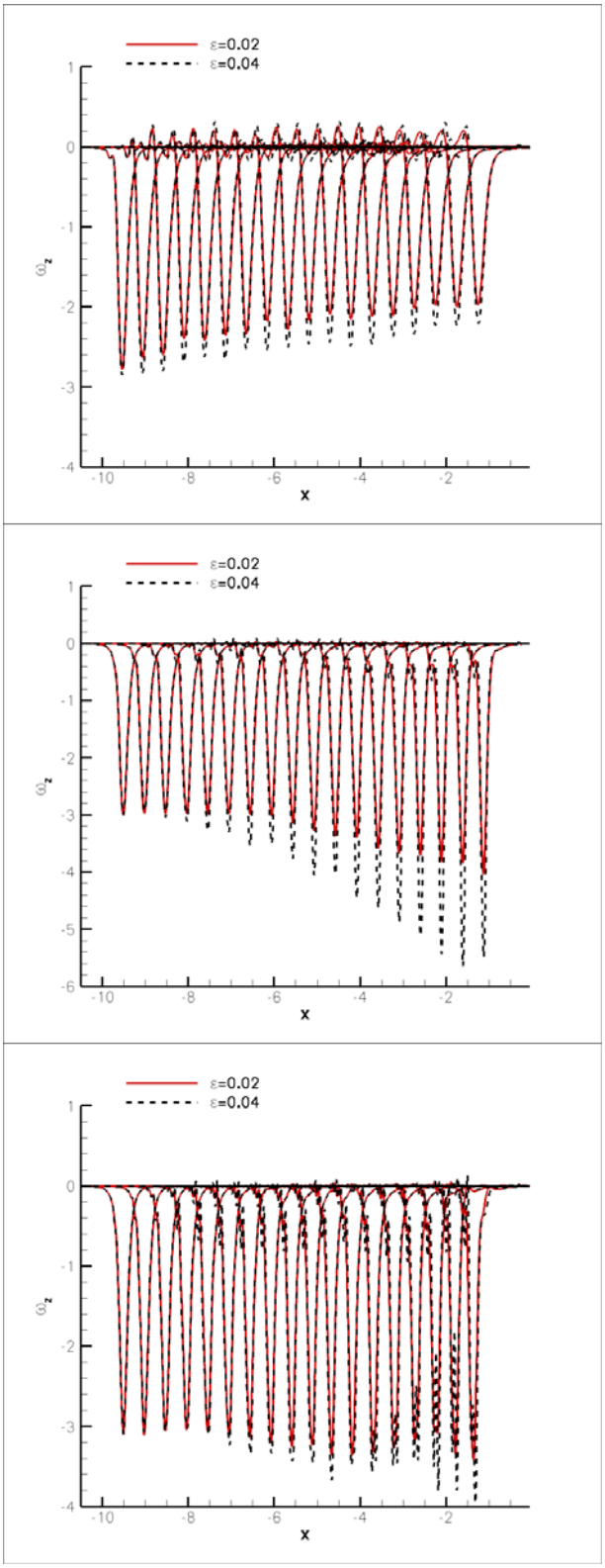

Figure 4: Vorticity profile across the vortex before the interaction with the original VC2 scheme – ε=0.02/0.04Δx, ε/μ=1.25– coarse mesh (top) – medium mesh (middle) – fine mesh (bottom)

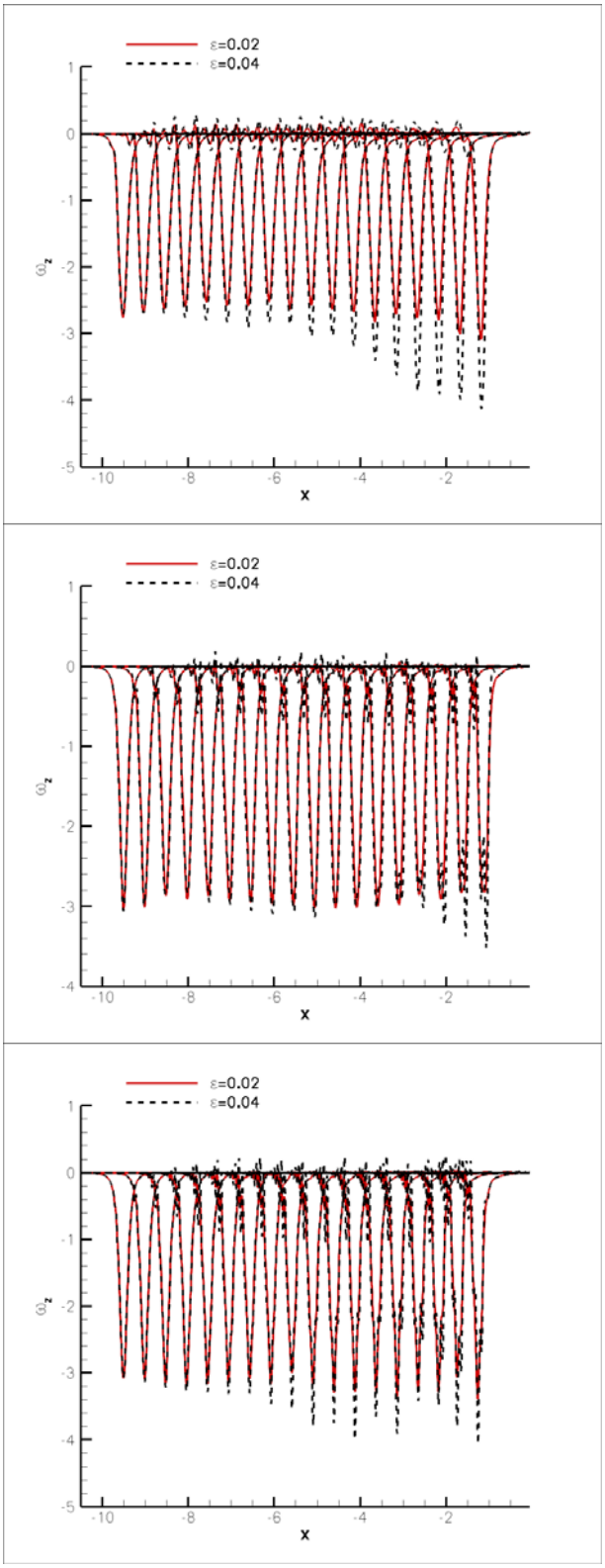

Figure 5: Vorticity profile across the vortex before the interaction with the 3rd-order VC2 scheme – ε=0.02/0.04Δx, ε/μ=1.25– coarse mesh (top) – medium mesh (middle) – fine mesh (bottom)

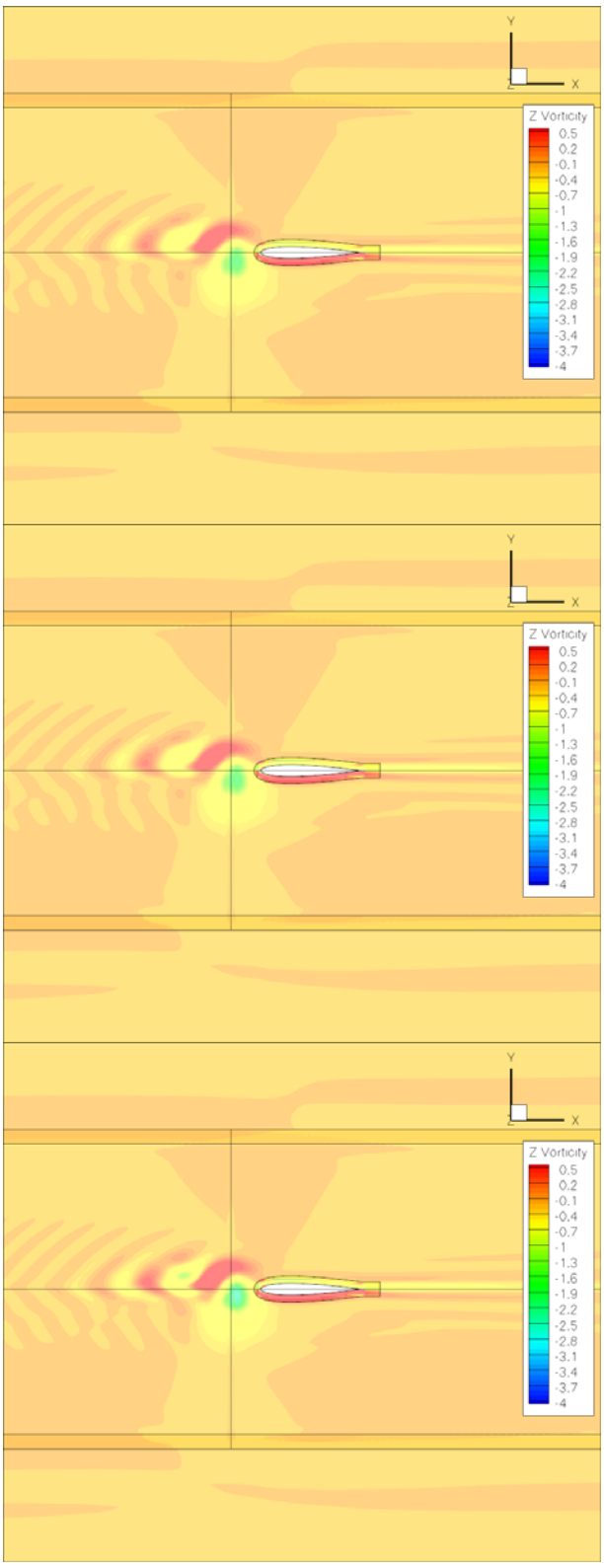

Figure 6: Effect of confinement parameter on vorticity at t=0 with the original VC2 scheme – ε/Δx =0 (top), 0.02 (middle), 0.04 (bottom) - ε/μ=1.25, coarse mesh

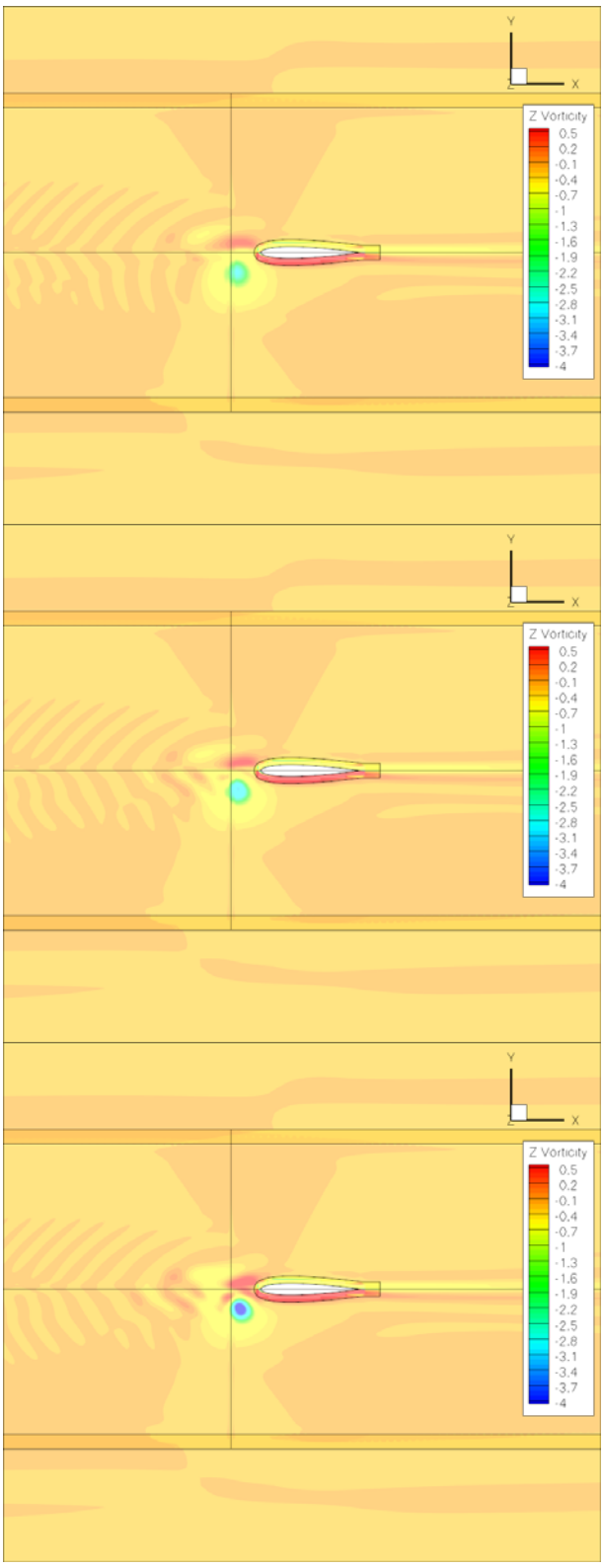

Figure 7: Effect of confinement parameter on vorticity at t=0 with the 3rd-order VC2 scheme – ε/Δx =0 (top), 0.02 (middle), 0.04 (bottom) - ε/μ=1.25, coarse mesh

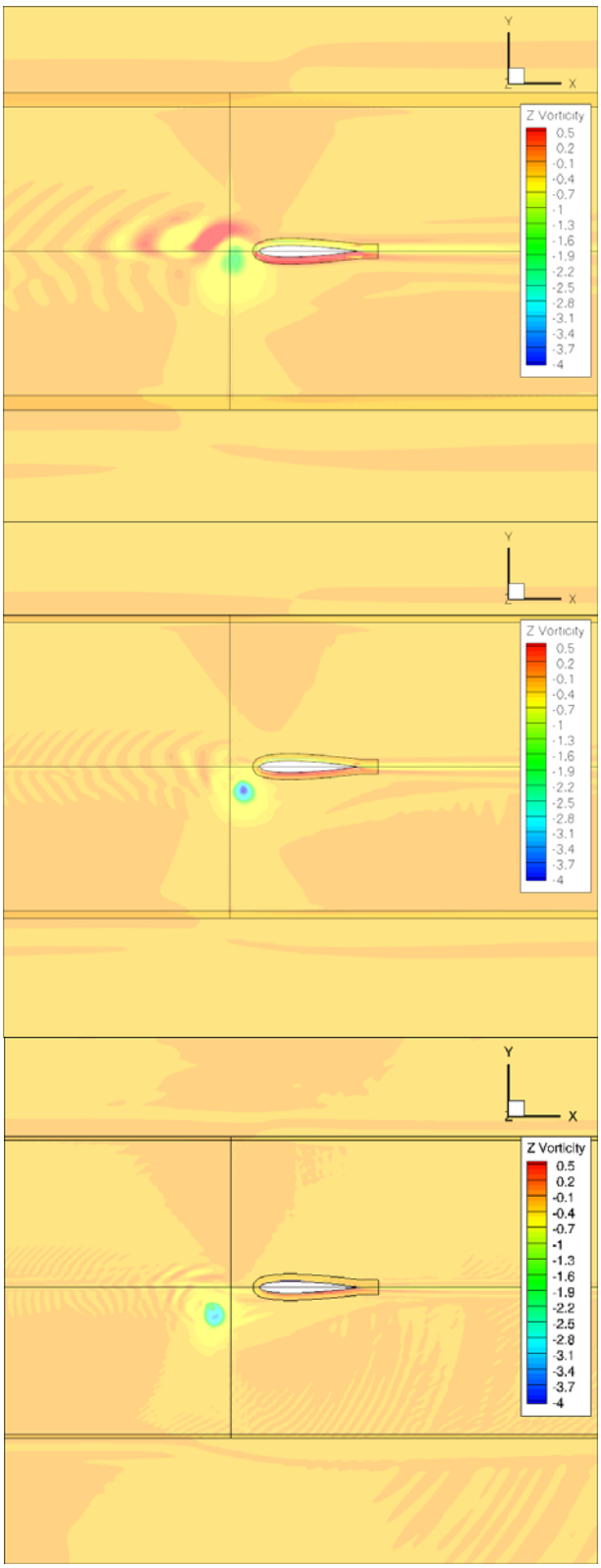

Figure 8: Effect of mesh fineness on vorticity at t=0 with the original VC2 scheme - coarse (top), medium (middle), fine mesh (bottom)– ε/Δx =0.02, ε/μ=1.25

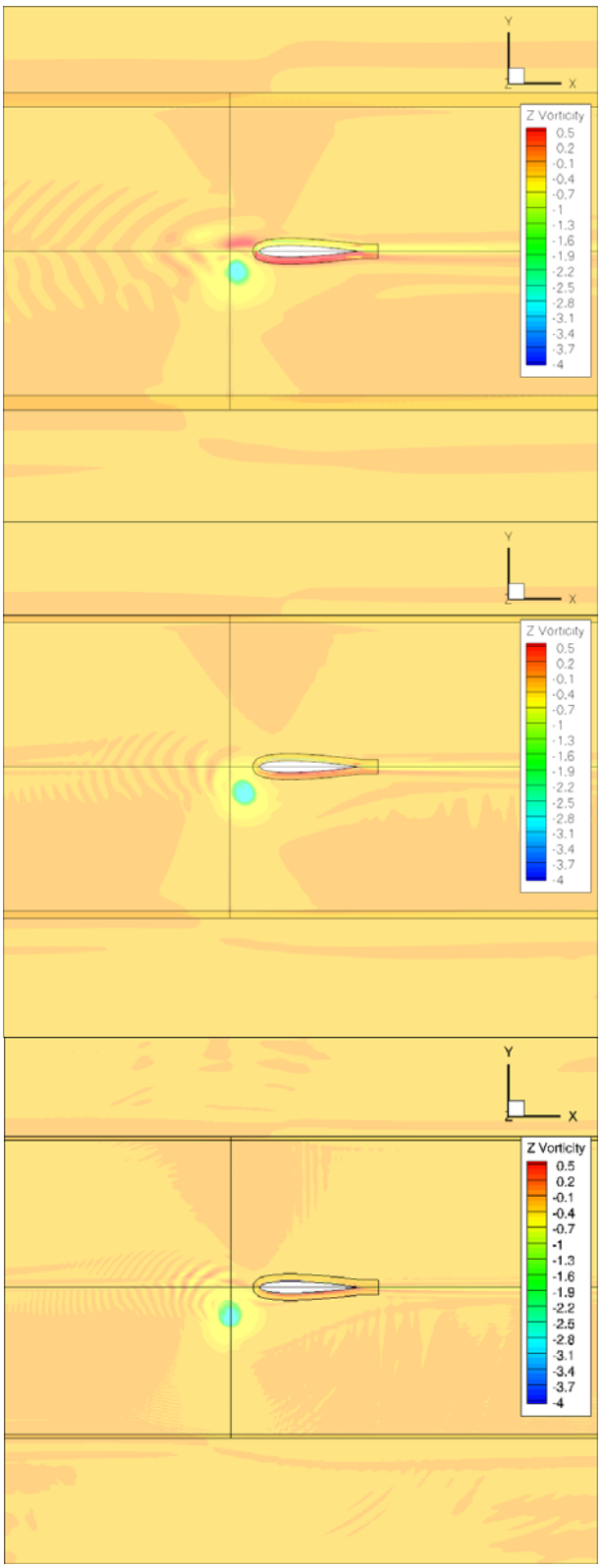

Figure 9: Effect of mesh fineness on vorticity at t=0 with the 3rd-order VC2 scheme - coarse (top), medium (middle), fine mesh (bottom)– ε/Δx =0.02, ε/μ=1.25

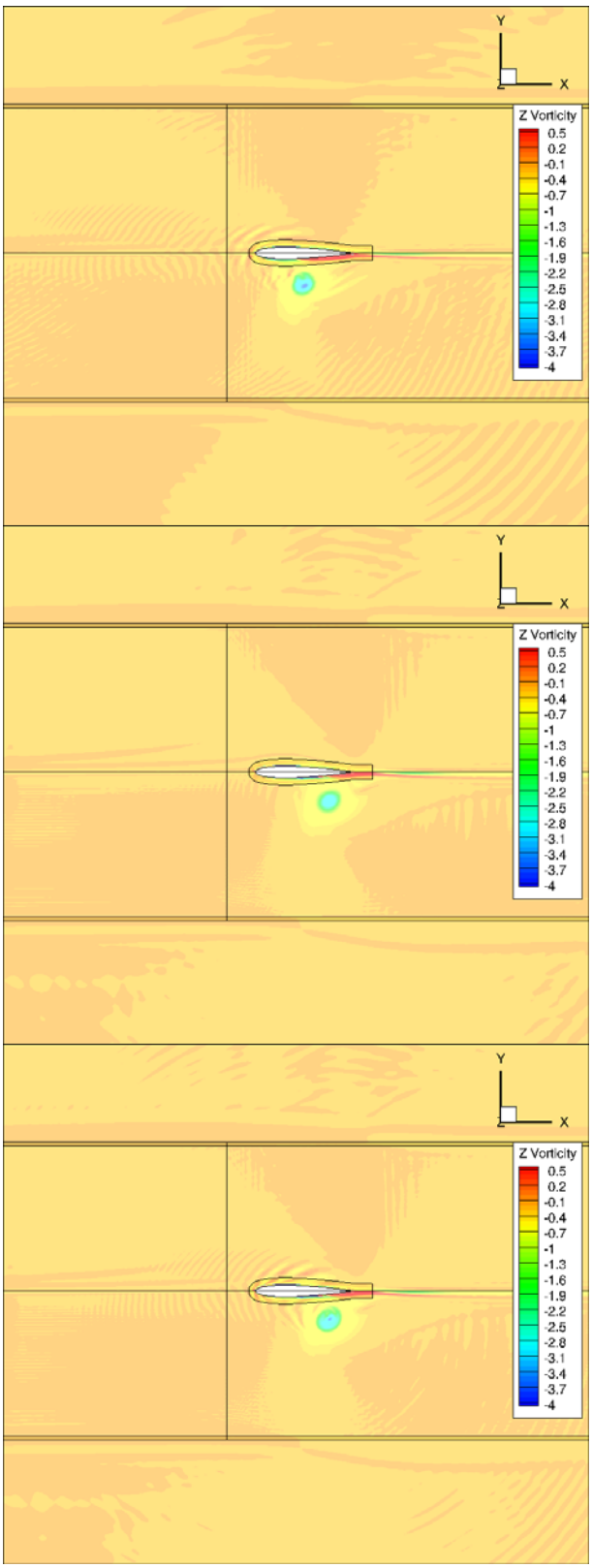

Figure 10: Vorticity at t=1 with the original VC2 (top), 3rd-order (middle), 3rd-order VC2 schemes (bottom) - fine mesh, ε/Δx =0.02, ε/μ=1.25

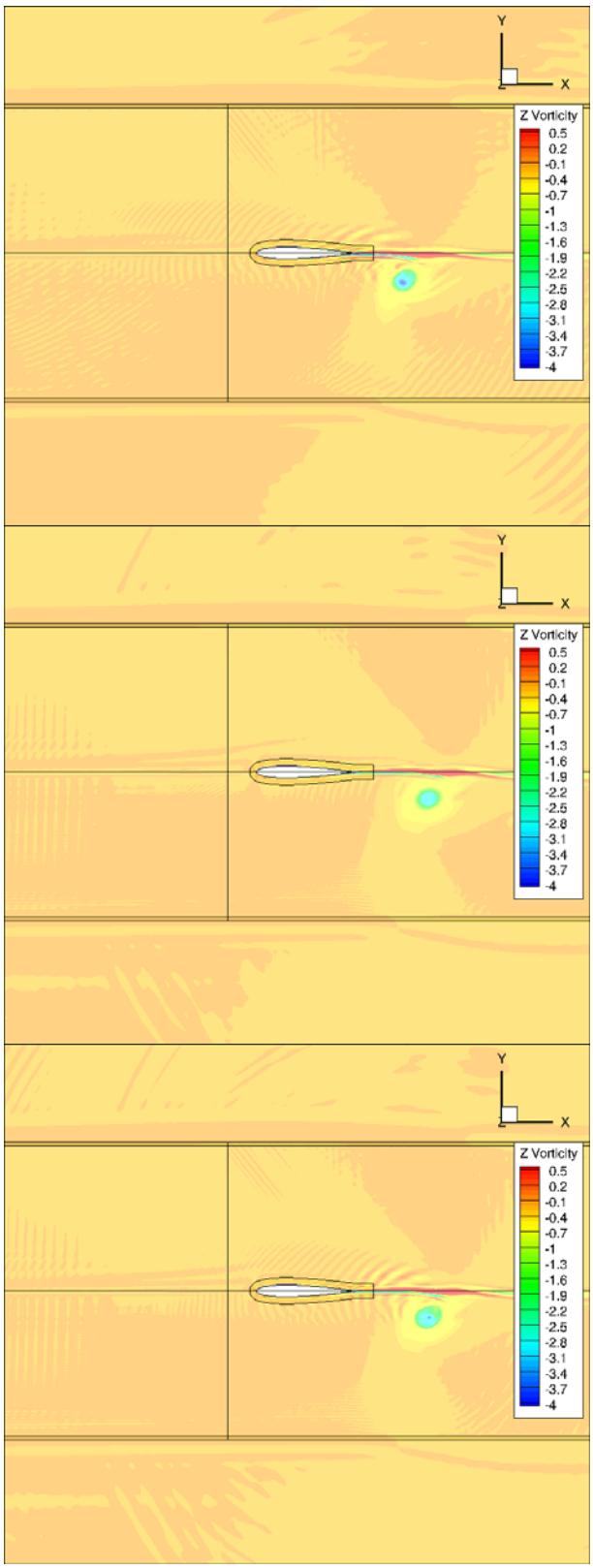

Figure 11: Vorticity at t=2 with the original VC2 (top), 3rd-order (middle), 3rd-order VC2 schemes (bottom) - fine mesh, ε/Δx =0.02, ε/μ=1.25

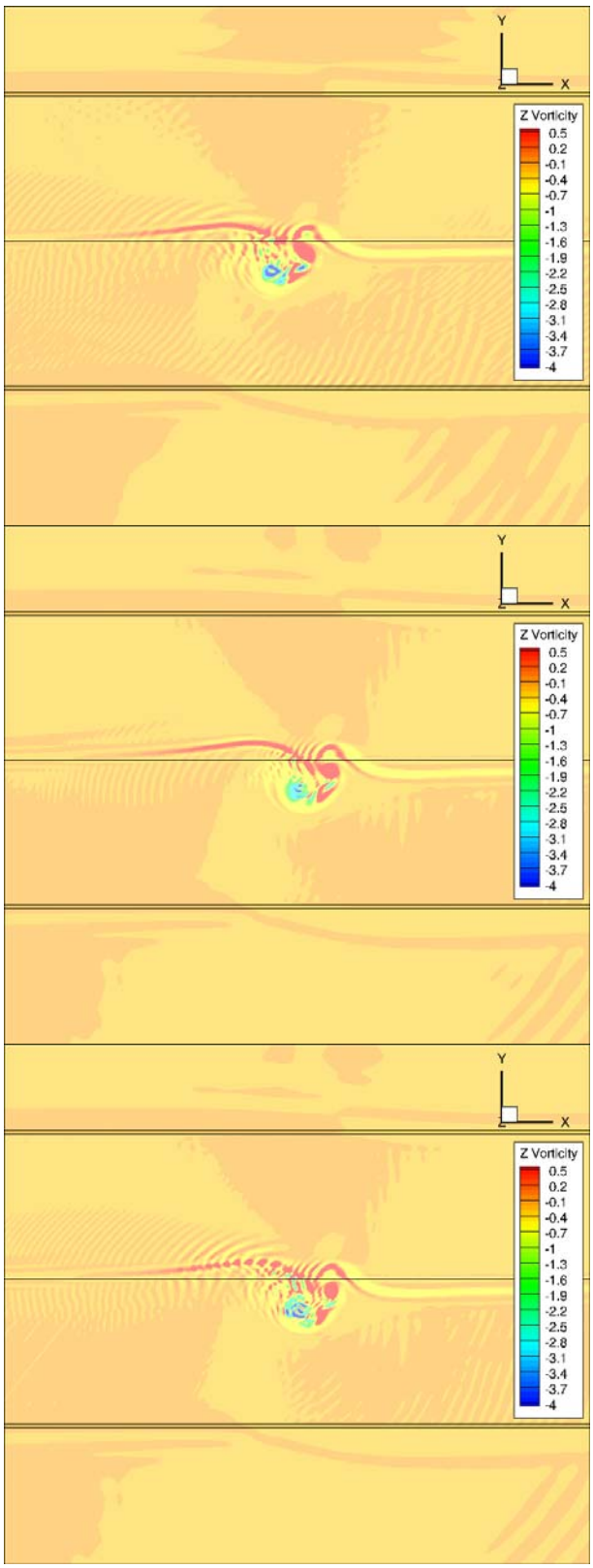

Figure 12: Vorticity at t=8 with the original VC2 (top), 3rd-order (middle), 3rd-order VC2 schemes (bottom) - fine mesh, ε/Δx =0.02, ε/μ=1.25

In order to better check it, the vorticity contours at reduced time t=0 are presented in Figure 6 for the original VC2 scheme and in Figure 7 for the 3rd-order VC2, using the coarse mesh simulations. Computations without confinement (ε/Δx =0), with ε/Δx =0.02 and 0.04, and a constant ratio ε/μ=1.25 are presented. With the 2nd-order scheme, the vortex has moved up and is about to hit the airfoil leading edge. Using VC2 slightly increases the intensity of the vortex but not its position. With the 3rd-order scheme, the vortex remains below the airfoil and has a more physical circular shape. In this case, introducing VC2 notably increases peak vorticity only when ε/Δx =0.04. At the same time of the simulation t=0, Figure 8 and Figure 9 present the effect of grid fineness on vorticity for a confinement parameter value of ε/Δx =0.02 only, using the 2nd-order and the 3rd-order scheme respectively. The too high position of the vortex computed with the 2nd-order scheme on the coarse mesh is no more visible with the medium and fine meshes. Furthermore, the higher peak vorticity at the vortex centre with the medium mesh is also clear. Finally, the difference in axial velocity of the vortex with mesh fineness can be noted. Similar features are obtained with the 3rd-order VC2, but the variation of the solution with mesh fineness is much smaller, indicating that the higher-order VC2 scheme is more accurate than the original one.

In Figure 10, a comparison of vorticity contours at reduced time t=1 is presented for the fine mesh and the simulation with the original VC2 scheme with 2nd-order Cartesian discretization, the 3rd-order scheme without confinement and the 3rd-order VC2 scheme. For the confined solutions, the same values of confinement parameters ε/Δx =0.02 and ε/μ=1.25 are used. The solutions are in fairly good agreement to one another. A layer of positive vorticity is developing in the rear part of the airfoil lower surface just above the vortex, due to the vortex passage. A slight difference in vortex speed can be observed between the 2nd-order and the 3rd-order schemes, without or with confinement, which may be attributed to a higher dispersion error. As a result, the layer of positive vorticity extends closer to the mid-chord of the airfoil with the 2nd-order scheme at this time of the simulation. Finally, both confined cases give a slightly higher peak vorticity inside the vortex than the one obtained without confinement, but the effect is moderate, especially with the 3rd-order confinement. The same comparison is presented at reduced time t=2 in Figure 11. The vortex is now located about 1 chord downstream the airfoil. The region of positive vorticity mentioned above has also been shed and goes with the vortex in the airfoil wake. Again, a good agreement between all solutions can be noted, with a slightly higher peak vorticity in the vortex core computed by the 2nd-order scheme with VC2. The same solutions are compared at time t=8 in Figure 12. The vortex is interacting with the positive vorticity pocket, providing a complex set of rotating structures. The solutions obtained with confinement match fairly well the 3rd-order one without confinement, with only small local differences due to the VC2 term which reduces the diffusion of vorticity.

These results thus show that the confinement terms do not modify the physics of the airfoil vortex-interaction. Furthermore, the solutions obtained with 3rd-order confinement are more accurate than those obtained with the original VC2 scheme, with a smaller dependency on the mesh fineness and on the confinement parameters and therefore a better correlation with the results computed with the 3rd-order scheme and the fine mesh.

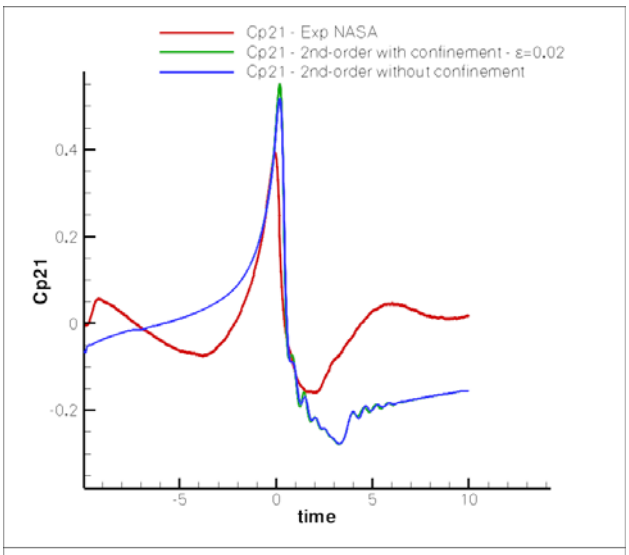

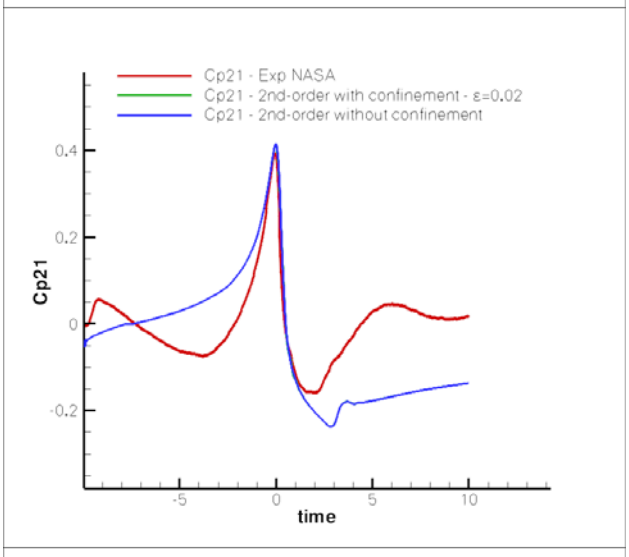

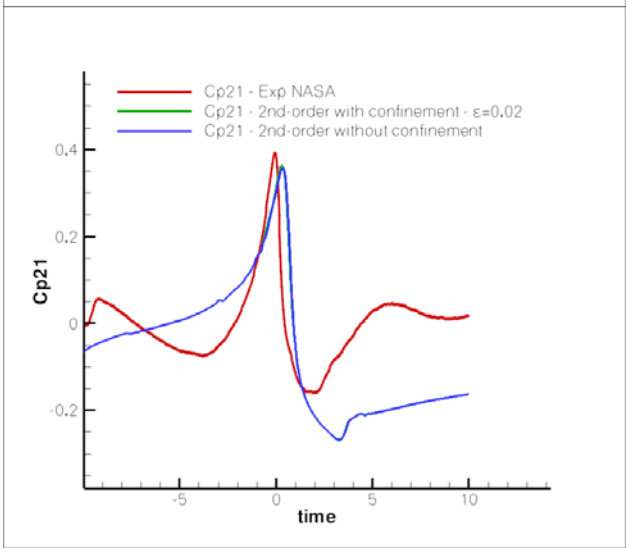

Figure 13: Effect of VC2 on upper surface pressure at x/c=2%, 2nd-order scheme, ε/Δx =0.02, ε/μ=1.25

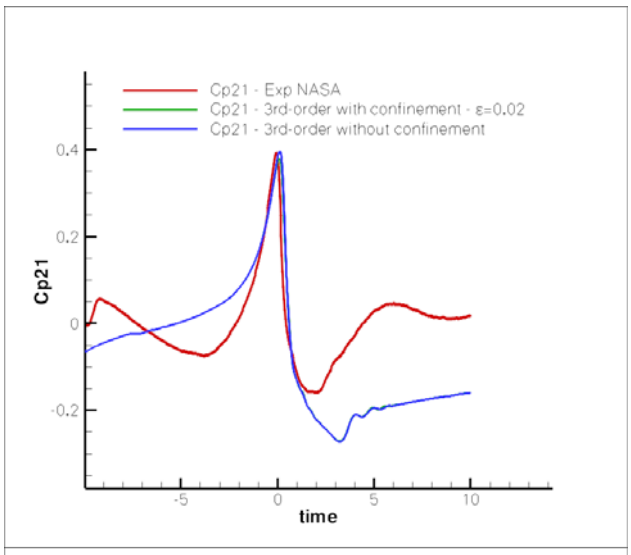

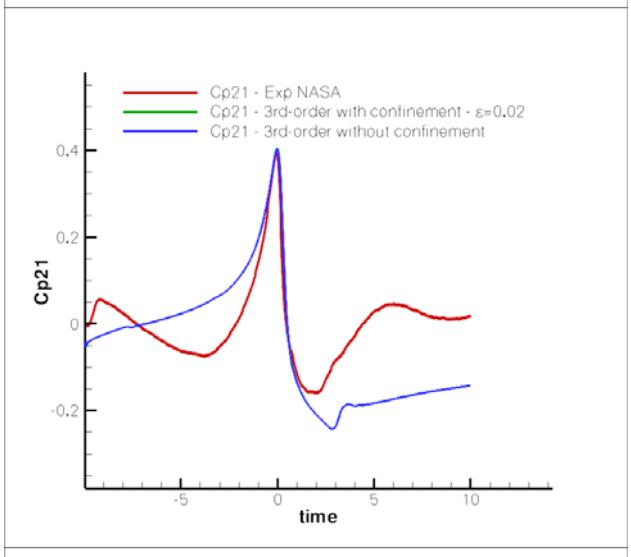

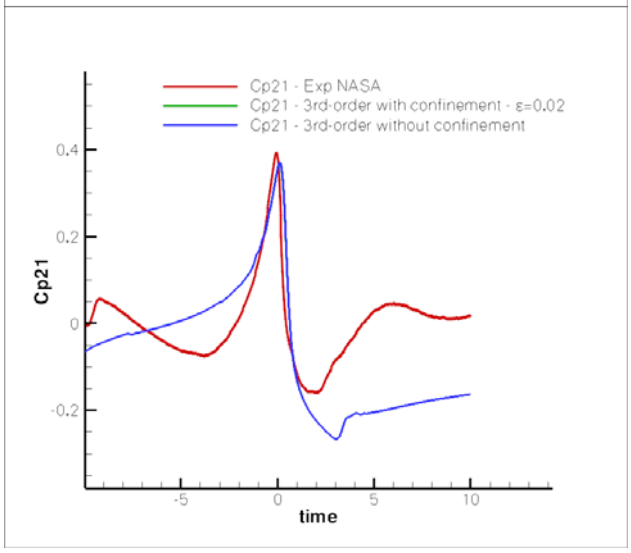

Figure 14: Effect of VC2 on upper surface pressure at x/c=2%, 3rd-order scheme, ε/Δx =0.02, ε/μ=1.25

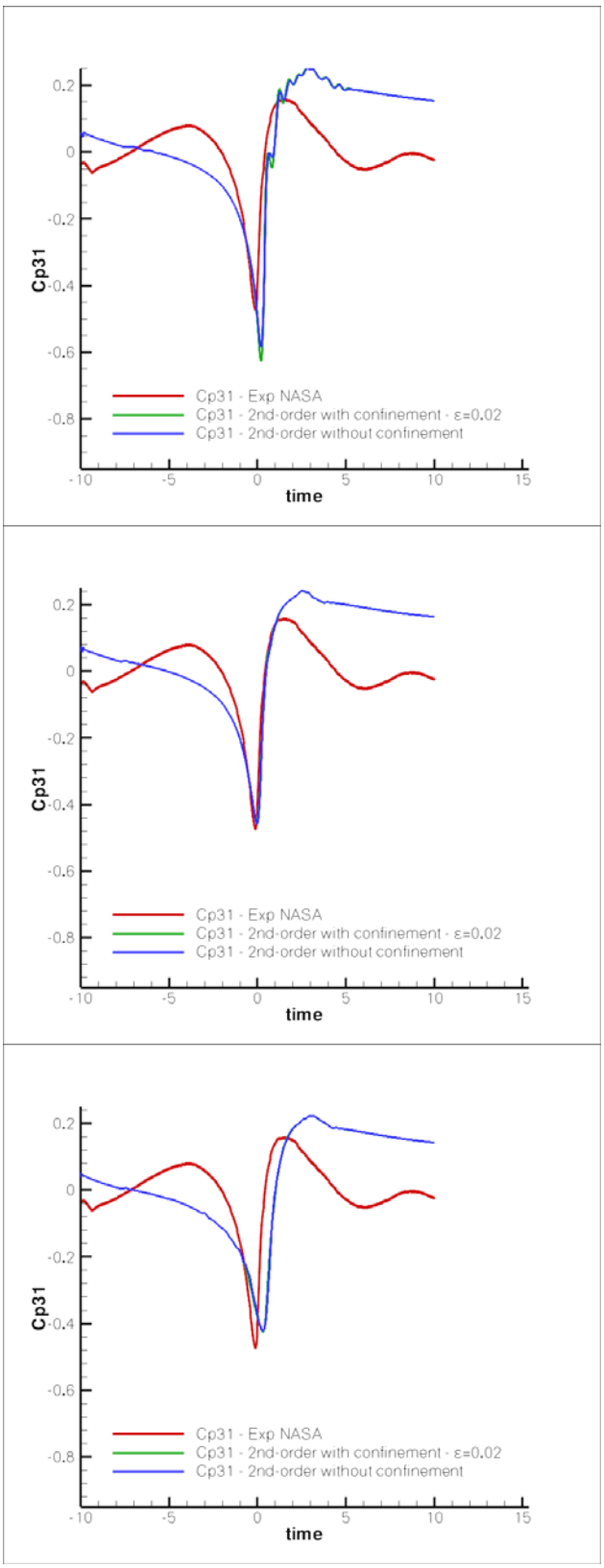

Figure 15: Effect of VC2 on lower surface pressure at x/c=2%, 2nd-order scheme, ε/Δx =0.02, ε/μ=1.25

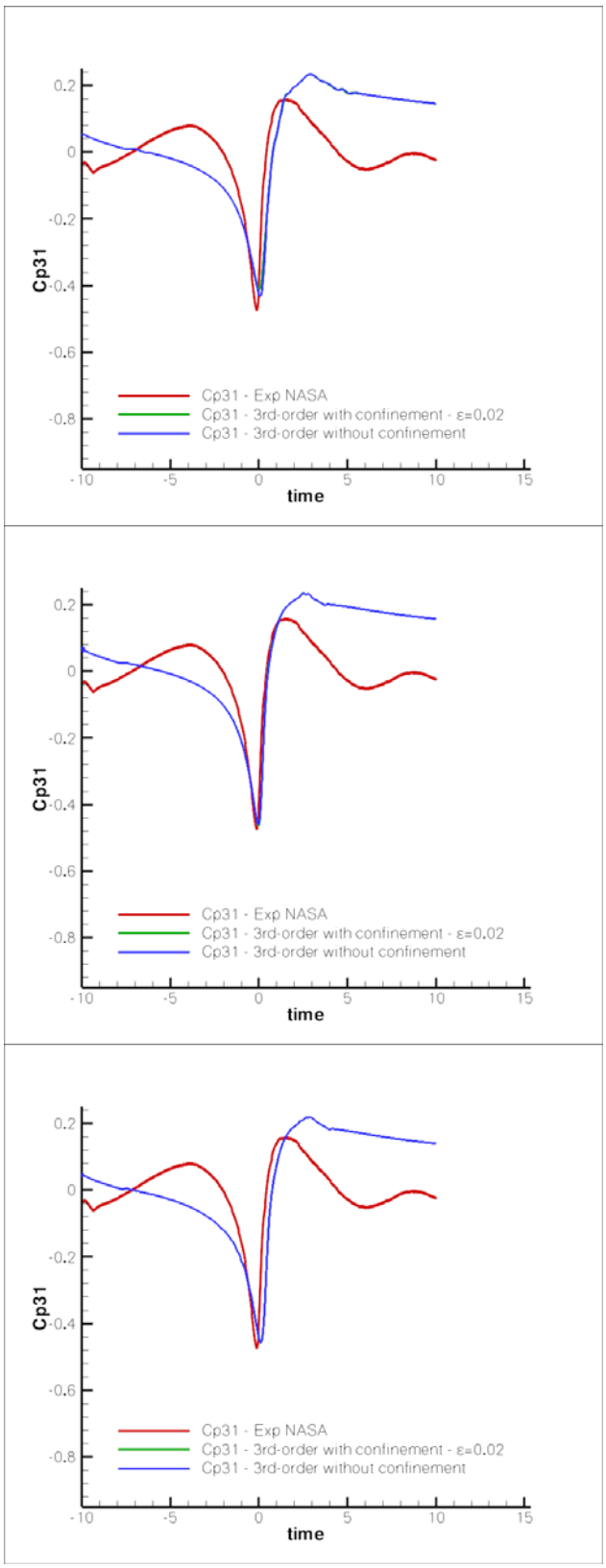

Figure 16: Effect of VC2 on lower surface pressure at x/c=2%, 3rd-order scheme, ε/Δx =0.02, ε/μ=1.25

It remains to check the effect of confinement on airfoil pressure evolution, which is at the source of the BVI noise. Similarly to the work presented in [9], we compare the computed time pressure evolution at the leading edge of the airfoil (x/c=2%) on the upper and lower surface, with

and without confinement. In order to get an idea of the physics and check that the computed data is qualitatively accurate, the experimental data measured by Kitaplioglu and Caradonna [10, 11] is plotted. As done in [9], the computed pressure coefficients are corrected in order to approximately match the 3D experiment at time t=-7. The upper surface pressure computed with the 2nd-order scheme, with and without VC2, with the 3 sets of meshes is presented in Figure 13. As expected, the effect of confinement is mainly noticeable for the coarse grid case where a collision between the vortex and the airfoil is obtained. The resulting interaction is much stronger than those computed with the medium and the fine grid, which show a fairly good correlation with experiment. Furthermore, by concentrating the vorticity inside the vortex core, the confinement increases the impulsivity of the interaction. The same comparison with the 3rd-order computations is plotted in Figure 14. In this case, the effect of confinement on airfoil pressure is quite small whatever the set of meshes used, and the correlation with experiment is satisfactory for all meshes computed. This low dependency of surface pressure to confinement is due to the good conservation of vorticity of the baseline schemes thanks to mesh fineness. It is also a clear indication that the VC2 confinement term does not introduce spurious vorticity in the simulation. The corresponding lower surface pressure evolutions are presented in Figure 15 and Figure 16 for the 2nd-order and 3rd-order computations respectively. Again, the only noticeable effect of confinement occurs with the 2nd-order simulation and the coarse mesh because of the airfoil-vortex collision. Elsewhere, the computed pressure is very weakly affected by confinement and matches reasonably well the experiment.

7A rotor in hover

The wake evolution of a simplified geometry of the 7A rotor in hover is considered here for an inviscid flow, solving the Euler equations. This case was already investigated in [7], as well as in [8] for a single blade configuration. The Chimera method is used again, with a curvilinear grid attached to each blade, all embedded in a set of Cartesian grids of various finenesses in order to cluster the number of points in the wake region. The cell size ratio between two adjacent grids is equal to 2 or 2.5. They communicate via the Chimera overset grids approach. All grids, curvilinear and Cartesian, have the same rotation velocity so that the computation of Chimera interpolation parameters can be frozen at the beginning of the run. The whole grid is much coarser than what was used in the previous example with a total number of cells of 3037720 for the whole rotor system (Figure 17). Steady-state solutions are investigated in the rotating frame, so that local time-stepping can be used with a CFL number equal to 20. For all cases, 24000 iterations are run and the solutions are compared in order to investigate the effect of numerical scheme and confinement on the wake. As will be seen, this may be a problem when the solution takes time to stabilize, which is more especially the case when a better preservation of rotor wake is obtained. Non-reflecting conditions are applied in the far-field boundaries in order to allow perturbations to get out of the computational domain. The same confinement parameters used for the previous BVI study are kept in order to check their correct scaling with mesh resolution: $\varepsilon/\mu=1.25$, $\varepsilon/\Delta x$ =0 (no confinement) / 0.02 / 0.04.

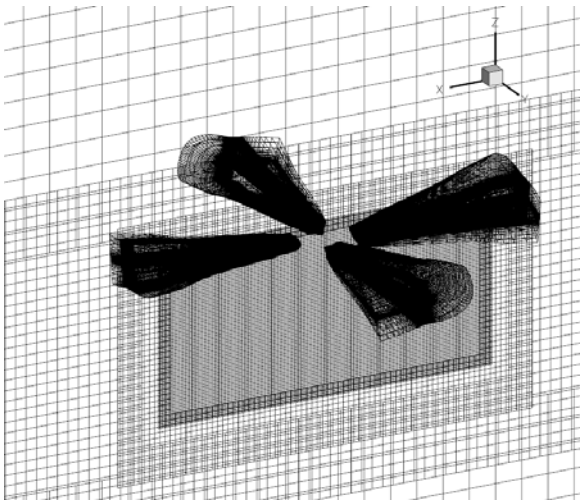

Figure 17: View of the Chimera mesh for the 7A rotor in hover

A cut across a wake diameter showing the vorticity contours is plotted in Figure 18 for the simulations with the 2nd-order scheme and the original VC2 method and in Figure 19 for the 3rd-order scheme with and without VC2. Again, the standard 2nd-order finite-volume scheme is applied on the curvilinear grids, whatever the method used on the Cartesian grids. The iso-surface of Q-criterion Q=0.1 is also plotted on these figures. The poor wake capturing capability of the original schemes without confinement was expected with such a coarse grid, and from this point of view the 3rd-order scheme does not better than the 2nd-order one. As a matter of fact, they have the same dissipation term coming from the explicit artificial viscosity and mainly differ from their dispersion error only. Introducing VC2 in the simulation improves the conservation of vortices in the wake. For the original VC2 method, the individual tip vortices show a regular pattern over more than 1.5 blade revolution, but their intensity is fairly low. On the contrary, the 3rd-order VC2 scheme shows better defined vortices with higher peak vorticity in their core. However, the wake looks more disorganized and unstable, so that hardly more than 1 wake revolution can be distinguished in the plotted results. When looking at the wake evolution over iterations (not presented here), the far wake is rolling up into a large “starting vortex”. This “super-vortex” is periodically shed downstream were it is diffused on the coarser mesh cells, but the process also induces perturbations in the near wake region and the computation does not converge towards a stable well-defined flow condition. The convergence process is also perturbed by the non-physical strong root vortices which are artificially created by the absence of rotor head in the simulation. Furthermore, in the present computations the blade roots are set at r/R=32% so that these artificial root vortices, when they are better captured in the simulations with confinement, tend to perturb the whole wake structure too much. Similar problems are also obtained with the 2nd-order scheme and the original VC2 method, but the solution finally stabilizes in the state shown here, probably because of a larger dissipation of the wake structures. Maybe the 3rd-order VC2 computations should be pursued longer in order to converge towards a steady-state. It is also known that the far-wake of a rotor in hover is unstable, and therefore it is also possible that the conservation of more concentrated vortices in the 3rd-order solution allows these instabilities to develop. In order to

check it, a time accurate simulation of the same configuration is required. A last point to be noted is that, for a fixed value of ε/μ, doubling the magnitude of the confinement parameters lead to more concentrated vortices in the solutions, quite in agreement with what was found for the airfoil-vortex interaction case above. Nevertheless, the solutions obtained are qualitatively very similar for all cases and the comments above apply for ε/Δx =0.02 and ε/Δx =0.04 as well.

The various wake geometries computed were extracted and compared using an analysis tool developed in-house [12]. In the present case, the technique proposed by Sujudi and Haimes [13], based on the eigenvectors of the velocity gradient, was applied to detect and locate vortices. The tip vortex geometry obtained from the various computations is shown in Figure 20 for the 2nd-order computations and in Figure 21 for the 3rd-order ones. They are classically presented in terms of wake contraction and axial convection. The wake instability discussed above with the 3rd-order VC2 scheme appears clearly with a slope discontinuity after one revolution, the vortex altitude remaining constant as a "super-vortex ring" afterwards. On the contrary, the 2nd-order scheme with confinement allows to follow the downstream convection of the tip vortex over almost 2 revolutions. However, the wake contraction computed with the 2nd-order scheme and VC2 is too large (close to 0.6) by comparison with the theoretical maximum contraction of $1/\sqrt{2}$, while the contraction computed with the 3rd-order scheme is too low (about 0.8) because of the perturbation introduced by the "super-vortex ring" downstream. It is also important to note that, for the part of the wake where the position of the tip vortex can be determined when no confinement is applied, the VC2 schemes, either original or 3rd-order accurate, do not modify its advection rate which is identical to the results obtained without confinement. Finally, the magnitude of the confinement parameters also does not modify the tip vortex geometry. These observations tend to show that the confinement terms do not modify the physics of the vortical flows developing around helicopter rotor blades in hover, and at least that their effect is of lower importance than that of the numerical scheme on the computed solution. In any case, the increased capability of confinement to maintain vorticity in the solution is beyond doubt.

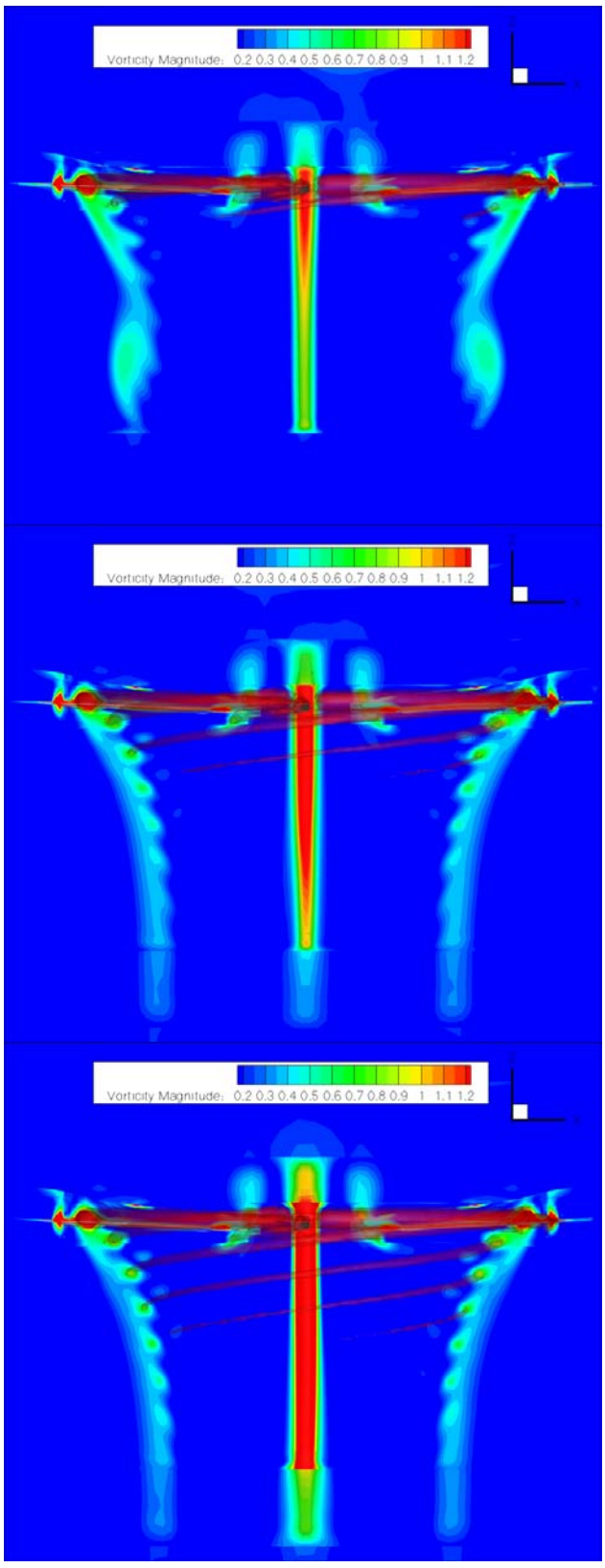

Figure 18: Effect of confinement parameter on vorticity contours and iso-surface of Q-criterion with the original VC2 scheme – ε/Δx =0 (top), 0.02 (middle), 0.04 (bottom), ε/μ=1.25

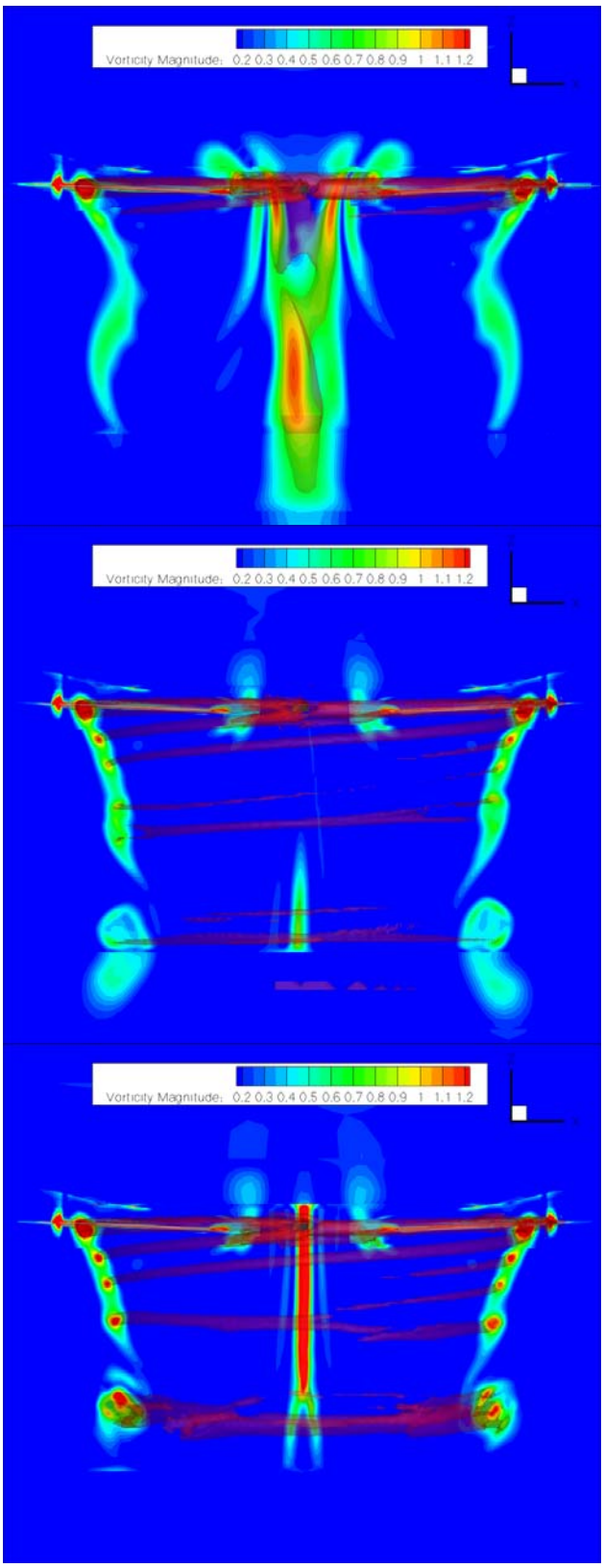

Figure 19: Effect of confinement parameter on vorticity contours and iso-surface of Q-criterion with the 3rd-order VC2 scheme – ε/Δx =0 (top), 0.02 (middle), 0.04 (bottom), ε/μ=1.25

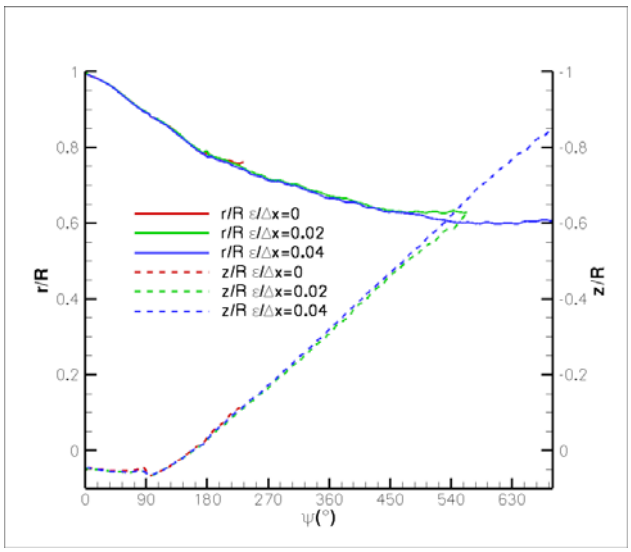

Figure 20: Effect of confinement on tip vortex geometry for the original VC2 scheme

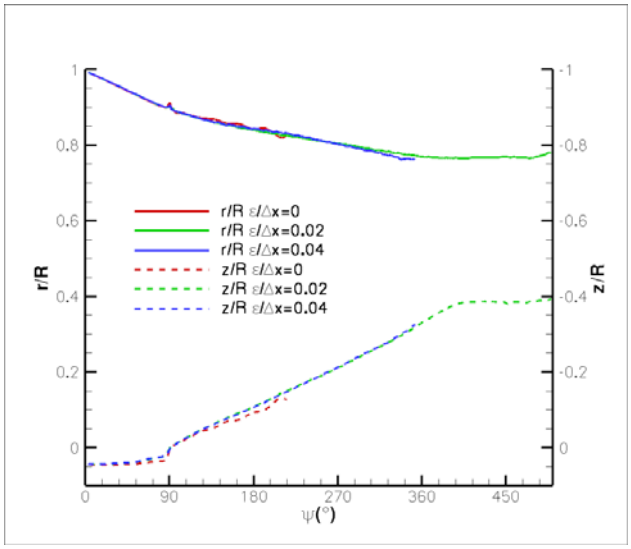

Figure 21: Effect of confinement on tip vortex geometry for the 3rd-order VC2 scheme (bottom)

CONCLUSIONS

A new 3rd-order Vorticity Confinement scheme based on the original VC2 method of Steinhoff has been developed for the Euler/RANS equations. It is an extension of similar developments for the 1D linear transport equation. The objective of this work is to get the capability to use confinement together with a higher-order discretization of the fluid dynamics equations. The higher-order accuracy is obtained by taking the Laplacian of the original VC2 term. The new scheme was tested by comparison with the original VC2 scheme and with the 3rd-order scheme without confinement for two inviscid flow configurations. The first test-case considered is a 2D airfoil-vortex interaction reproducing the conditions of the Kitaplioglu-Caradonna experiment for a blade section located at 87.6% of the radius. A grid sensitivity study was performed, using 3 sets of grids of increasing fineness capable to discretize the vortex core accurately, using the same vorticity confinement parameters. The results

obtained show that the 3rd-order confinement combines the benefits of the higher-accuracy of the 3rd-order scheme with the confinement capability of the original VC2 scheme. The new solutions have a smaller sensitivity to the grid fineness than the original VC2 ones and reproduce well the flow features computed by the 3rd-order scheme with the finest mesh. The second test case considered concerns a simplified configuration of the 7A rotor in hover computed with a coarse grid. The computations with confinement were run using the same confinement parameters applied above. Both original and 3rd-order VC2 schemes improve the wake conservation capability of the baseline 2nd-order and 3rd-order schemes. The better preservation of the tip vortex structure with the 3rd-order confinement with respect to the original VC2 could also be observed. However, the more concentrated vortices obtained also generate wake instabilities which do not allow to follow the tip vortex trajectory over a so long period of time as that obtained with VC2. Further work is required in order to understand whether this instability is of physical or numerical origin.
On the whole, the new higher-order VC2 scheme follows our expectations by combining accuracy and anti-diffusivity. A deeper validation of the methodology is necessary. Finally, the procedure adopted in the present work can also be extended to higher-orders.

Acknowledgements

This work was completed in the frame of the SHANEL project funded by French Ministry of Transport (DGAC) and monitored by Ministry of Defence (DGA). The author also wants to acknowledge Stéphanie Peron, Christophe Benoit and Pascal Raud from the DSNA Department of ONERA, and Benoit Rodriguez from the DAAP Department, for their support in the developments in the Cassiopée solver. Stéphanie Peron also provided all the data necessary for running the BVI test case. Enric Roca Leon, PhD student at Eurocopter and at the DAAP Department also provided precious support for using the wake analysis tool.

References

1. Steinhoff, J., Lynn, N., “Treatment of vortical flows using vorticity confinement”, Chapter 10 of Computing the Future IV : Frontiers of Computational Fluid Dynamics, Ed. by Caughey, D.A. & Hafez, M.M., Springer-Verlag, 2006.

2. Costes, M., Kowani, G., “An automatic anti-diffusion method for vortical flows based on Vorticity Confinement”, Aerospace Science and Technology No 7 (2003), pp. 11-21.

3. Costes, M., “Analysis of the second vorticity confinement scheme”, Aerospace Sciences and Technology, Vol. 12/3 pp 203-213, April 2008.

4. Steinhoff, J., Puskas, E., Babu, S., Wenren, Y., Underhill, D., “Computation of thin features over long distances using solitary waves“, AIAA paper 97-1976, 13th Computational Fluid Dynamics Conference, Snowmass, Colorado, June 1997.

5. Steinhoff, J., Dietz, W., Haas, S., Xiao, M., Lynn, N., Fan, M., “Simulating small scale features in fluid dynamics and acoustics as nonlinear solitary waves”, AIAA paper 2003-078, 41st Aerospace Meeting and Exhibit, Reno, Nevada, January 2003.

6. Costes, M., Juillet, F., “Analysis and higher-order extension of the VC2 confinement scheme”, Computer & Fluids 56 (2012), 102-117.

7. Costes, M., Renaud, T., Rodriguez, B., Reboul, G., “Application of vorticity confinement to rotor wake simulations”, Int. J. Engineering Systems Modelling and Simulation, Vol. 4, Nos. 1/2, 2012.

8. Saunier, O., Peron, S., Jeanfaivre, G., Benoit, C., Lerat, A., “High-order accurate Cartesian partitioning methods. Application to rotor flows”, 33rd European Rotorcraft Forum, Kazan, Russia, September 2007.

9. Peron, S., Benoit, C., Renaud, T., Sidès, J., Tanabe, Y., Saito, S., Yang, C., Aoyama, T., “ONERA/JAXA common investigations on CFD tools for an accurate prediction of BVI”. AHS Specialists Meeting, Seoul, Korea, October 2007.

10. Kitaplioglu, C., Caradonna, F.X., “Aerodynamics and acoustics of blade-vortex interaction using an independently generated vortex”, AHS Specialists Conference, San Francisco, California, January 1994.

11. Kitaplioglu, C., Caradonna, F.X., Burley, C.L., “Parallel blade-vortex interactions: an experimental study and comparison with computations”, Journal of the AHS, Vol. 42, No. 3, pp. 272-281, July 1997.

12. Roca Leon, E., “On the definition and characterization of vortices”, Master Thesis Report, ISAE, September 2010.

13. Sujudi, D., Haimes, R., “Identification of swirling flow in 3D vector fields”, Technical Report, Dep. of Aeronautics and Astronautics, MIT, 1995.